THE INSULIN-LIKE GROWTH FACTOR I RECEPTOR REGULATES GLUCOSE TRANSPORT BY ASTROCYTES

Edwin Hernandez-Garzón[1,2*], Ana M. Fernandez[1,2*], Alberto Perez-Alvarez[1,3], Laura Genis[1,2], Pablo Bascuñana[4], Ruben Fernandez de la Rosa[4], Mercedes Delgado[4], Miguel Angel Pozo[4], Estefania Moreno[2,5], Peter J. McCormick[2,5,6], Andrea Santi[1,2], Angel Trueba-Saiz[1,2], Cristina Garcia-Caceres[7], Matthias H. Tschöp[7], Alfonso Araque[1], Eduardo D. Martin[8], and Ignacio Torres Aleman[1,2]

[1]Cajal Institute, CSIC, Madrid 28002, Spain. [2]Ciberned, Spain. [3]Eppendorf Center for Molecular Neurobiology Hamburg, D-20251, Germany. [4]Pluridisciplinary Institute, Complutense University, Madrid 28040, Spain. [5]Dept Biochemistry and Molecular Biology, University of Barcelona, Barcelona 08007, Spain. [6]School of Pharmacy, University of East Anglia, Norwich, Norfolk NR4 7TJ, UK; [7]Institute for Diabetes and Obesity, Munich D-85748, Germany, and [8]Science and Technology Park, Institute for Research in Neurological Disabilities, University of Castilla-La Mancha, Albacete 02071, Spain.

Correspondence to: Ignacio Torres Aleman. Cajal Institute. Avda Dr Arce 37, Madrid 28002. Spain

Main points:

- IGF-IR modulates glucose transport in astrocytes
- IGF-IR retains astrocytic GLUT1 inside the cell
- IR and IGF-IR play opposite roles in GLUT1 activity in astrocytes

Key words: astrocytes, insulin like growth factor I receptor, glucose metabolism, glucose transporter 1
Running title: Insulin-like growth factor I receptor and brain glucose
Total number of words: 6,744
Abstract: 175; Introduction: 289; Materials and Methods: 2,253; Results: 1,032; Discussion: 531; References: 939; Legends: 1,146
Number of Figures: 5
Number of Tables: 0

*These authors contributed equally to this work

Abstract

Previous findings indicate that reducing brain insulin-like growth factor I receptor (IGF-IR) activity promotes ample neuroprotection. We now examined a possible action of IGF-IR on brain glucose transport to explain its wide protective activity, as energy availability is crucial for healthy tissue function. Using ^{18}FGlucose PET we found that shRNA interference of IGF-IR in mouse somatosensory cortex significantly increased glucose uptake upon sensory stimulation. In vivo microscopy using astrocyte specific staining showed that after IGF-IR shRNA injection in somatosensory cortex, astrocytes displayed greater increases in glucose uptake as compared to astrocytes in the scramble-injected side. Further, mice with the IGF-IR knock down in astrocytes showed increased glucose uptake in somatosensory cortex upon sensory stimulation. Analysis of underlying mechanisms indicated that IGF-IR interacts with glucose transporter 1 (GLUT1), the main facilitative glucose transporter in astrocytes, through a mechanism involving interactions with the scaffolding protein GIPC and the multicargo transporter LRP1 to retain GLUT1 inside the cell. These findings identify IGF-IR as a key modulator of brain glucose metabolism through its inhibitory action on astrocytic GLUT1 activity.

Introduction

Reduction of brain IGF-IR activity provides salutary effects. Intriguingly, neuroprotective actions of lowered brain IGF-IR encompass a wide variety of insults of different etiology (Biondi et al. 2015; Cohen et al. 2009; De Magalhaes Filho et al. 2016; Gontier et al. 2015), and even prolong lifespan (Kappeler et al., 2008). While diverse mechanisms have been invoked to explain the ample spectrum of beneficial actions of reduced IGF-IR activity (Gazit et al. 2016; Kenyon 2010; Lopez-Otin et al. 2013; Vilchez et al. 2014), it is possible that IGF-IR targets additional mechanisms of wide functional impact such as energy balance, as insulin-like receptors and their ligands are well known modulators of glucose and lipid handling in different tissues and species.

Conversely, IGF-I, the preferred ligand of IGF-IR, is generally considered a neuroprotective factor and has been proposed as a treatment for various neurodegenerative diseases (Fernandez and Torres-Aleman 2012) . This poses the paradox that either increasing IGF-I or reducing its receptor appears to lead to beneficial actions in the brain (Cohen and Dillin 2008; Fernandez and

Torres-Aleman 2012). While these apparently contradictory observations remain largely unexplained (but see (O'Neill et al., 2012), one possibility is that IGF-IR has ligand independent actions, as recently reported for apoptotic signaling through insulin receptor (IR) and IGF-IR (Boucher et al., 2010).

In the present work we analyzed a possible involvement of the IGF-I receptor on glucose handling by the brain, a key aspect in tissue homeostasis that could in theory form part of neuroprotection by insulin-like receptors, but remains little explored. We now describe that the IGF-I receptor inhibits in a ligand-independent manner the activity of glucose transporter 1 (GLUT1) in astrocytes, adding further support for a broad beneficial effect of reducing brain IGF-IR levels.

Materials and Methods

Animals

Adult (3-5 months old) and neonatal C57BL6/J mice were used. Mutant mice with reduced levels of IGF-IR in astrocytes (AsIGF-IR $^{+/-}$) were obtained by crossing IGF-IR$^{floxP/floxP}$ mice (the IGF-IR gene flanked by LoxP sites; Jackson Labs) with GFAP-Cre mice (Cre expression under the human GFAP promoter; Jackson Labs), both in a C57BlJ background. Littermates with IGF-IR$^{flox/flox}$, IGF-IR $^{flox/-}$, and IGF-IR$^{+/+}$ Cre$^{+/?}$ were pooled and used as controls. GFAP-Cre mice crossed with Rosa26 tomato-eGFP (a reporter mouse line from Jackson Labs) mice express GFP in astrocytes, whereas AsIGF-IR$^{-/-}$ mice expressed Cre in astrocytes (not shown). While levels of IGF-IR in the brain of AsIGF-IR $^{-/-}$ mice were significantly reduced (see below), levels of insulin receptor were normal (not shown). Animals were genotyped by PCR using primers for GFAP-Cre forward: ACT CCT TCA TAA AGC CCT and reverse: ATC ACT CGT TGC ATC GAC CG, and for IGF-IR forward: CTT CCC AGC TTG CTA CTC TAG G and reverse: CAG GCT TGC AAT GAG ACA TGG G. Two other transgenic mice lines (hGFAP-CreERT2 and IR$^{loxP/loxP}$ mice) were crossed to obtain GFAPIR-KO mice lacking IR in astrocytes when injected with tamoxifen, as explained in detail elsewhere (Garcia-Caceres et al. submitted). hGFAP-CreERT2 mice, an inducible transgenic mouse line under the control of a GFAP promoter and estrogen (C57BL/6J background, FM Vaccarino, Yale University School of Medicine) were mated with IR$^{loxP/loxP}$ mice (generated by R Kahn, Joslin Diabetes Center), and breeding cages were maintained by mating IR$^{loxP/loxP}$ and IR$^{loxP/loxP}$;hGFAP-CreERT2 mice. To excise loxP sites

by Cre recombination, 6 weeks-old male mice were administrated a daily tamoxifen injection (10 mg/kg, intraperitoneal) for 5 days. Tamoxifen (Sigma) was dissolved in sunflower oil at a final concentration of 10 mg/ml at 37º, and then filter sterilized and stored for up to 7 days at 4ºC in the dark. $IR^{loxP/loxP}$ mice were used as controls and also were injected with tamoxifen. PCR genotyping was carried out using primer sets binding to Cre (Cre-1084, 5´- GCG GTC TGG CAG TAA AAA CTA TC-3´; Cre-1085, 5´- GTG AAA CAG CAT TGC TGT CAC TT-3´; Cre-42, 5´-CTA GGC CAC AGA ATT GAA AGA TCT-3´; Cre-43, 5´-GTA GGT GGA AAT TCT AGC ATC ATC C-3 and crossing the loxP site (oKAHN03: 5- GAT GTG CAC CCC ATG TCT G-3´; oKAHN04: 5-TCT ATC AAC CGT GCC TAG AG-3´; oKAHN05: 5-CTG AAT AGC TGA GAC CAC AG-3´). Animal procedures followed European (86/609/EEC & 2003/65/EC, European Council Directives) guidelines and studies were approved by the respective local Bioethics Committees. All in vivo experiments were done blinded.

Plasmid Constructions and viral packaging

For viral transduction we used a three-plasmid system previously described (Dull et al. 1998). The co-transfection system consisted of an shRNA plasmid against either IGF-IR or IR (also used for transfecting primary astrocyte cultures), a packaging construct (pCMV-dR8.2 Δvpr) and the vesicular stomatitis virus G-protein envelope (pMD2.G, Addgene, USA). shRNAs against Glut-1, IGF-IR, IR, scramble sequence and EGFP were from Origene (HuSH-29, Origene, USA): shRNA against GIPC was constructed as described in www.addgene.org/tools/protocols/plko/ using the primers: 5'CCGGACTCACCGA ACCTCGGAAGGCCTCGAGGCCTTCCGAGGTTCGGTGAGT TTTTTG3' and 5'AATTCAAAAAACTCACCGAACCTCGGAAGGCCTCGAGGCCTTCCGAGG TTCGGTGAGT3' directed against the 684-704 fragment of GIPC mRNA. The transfer vector (5 μg), the envelope (2 μg), and the packaging plasmids (5 μg) were co-transfected using calcium phosphate in human embryonic kidney 293 T cells (6 × 106 cells per dish) cultured in DMEM with 10% FCS and 1% penicillin/streptomycin. Lysosomal function was inhibited with cloroquine prior to transfection. The supernatant containing the viral particles was collected, filtered and stored at −80°C until use. Viral concentration was titrated as described (Munive et al. 2016). Infection efficiency was ~80% as determined using GFP-expressing viral particles. shLRP-1 was obtained as described (Nishijima et al. 2010). GLUT1-Exo Flag was a kind gift of JC Rathmell (Wieman et al. 2007).

Cell cultures and transfections

Astroglial cultures with >95% GFAP-positive cells were prepared as described (Fernandez et al. 2007). Postnatal (day 3–4) brains from wild type, mutant As IGF-IR , and littermate mice were dissected and immersed in ice-cold Hank's balance salt solution (HBSS, Life Technologies, Spain). Cortex and hippocampus were removed and mechanically dissociated. The resulting cell suspension was centrifuged and plated in DMEM/F-12 (Life Technologies) with 10% fetal bovine serum (Life Technologies) and 100 mg/ml of antibiotic-antimycotic solution (Sigma-Aldrich). After 15–20 days, astrocytes were re-plated at 1.2×10^5 cells/well. For transfection, astrocytes were electroporated (2×10^6 astrocytes with 2 µg of plasmid DNA) before seeding using an astrocyte Nucleofector Kit (Amaxa, Lonza, Switzerland). After electroporation, cells were plated to obtain a final cell density on the day of the experiment similar to that obtained with the transfection method. The transfection efficiency was 60–80%, as assessed with a GFP vector.

Glucose assays

We used 6-NBDG to measure glucose transport in astrocytes as shown by others (Barros et al. 2009a). Briefly, cells well starved in serum free media for 3 hours. Then IGF-I (PreProTec, UK), insulin (Sigma, USA), or vehicle were added to a final concentration of 1nM. We then added 6-NBDG (Setareh biotech, USA) to a final concentration of 30 µM. Cultures were kept for 3 hours at 37°C and then ice cold PBS was added and cells trypsinized. Cells were collected and FBS and PBS added. Fluorescence intensity was measured by flow cytometry (FACSAria cytometer, BD Biosciences, USA).

***In Situ* Proximity Ligation Assays (PLA)**

GLUT1 – IGF-IR interactions were detected in astrocytes grown on glass coverslips using the Duolink II in situ PLA detection Kit (OLink; Bioscience, Sweden) as previously described (Gonzalez et al. 2012). Astrocytes were fixed in 4% paraformaldehyde for 10 min, washed with PBS containing 20 mM glycine to quench the aldehyde groups, permeabilized with the same buffer containing 0.05% Triton X-100 for 5 min and successively washed with PBS. After 1 h/37°C with the blocking solution in a pre-heated humidity chamber, astrocytes were incubated overnight with primary antibodies: rabbit polyclonal anti-GLUT1 antibody (1:100, ref. sc-7903; Santa Cruz Biotechnology) and monoclonal mouse anti-IGF-I receptor antibody (1:100, ref. sc-463; Santra Cruz Biotechnology) and were processed following the instructions of the supplier

using the PLA probes detecting rabbit or mouse antibodies (Duolink II PLA probe anti-Rabbit plus and Duolink II PLA probe anti-Mouse minus diluted in antibody diluent to a concentration of 1:5) and a DAPI-containing mounting medium. Samples were observed in a Leica SP2 confocal microscope (Leica Microsystems, Germany) equipped with an apochromatic 63X oil-immersion objective. For images of each field a maximum projection (superimposed sections) in two channels (one per staining) of 6 to 12 Z stacks with a step size of 1 µm were acquired.

Protein Translocation Assay

Translocation of GLUT1-Flag and IGF-IR to the cell membrane was evaluated following previously published procedures (Koshy et al. 2010). In brief, cultured astrocytes were labeled with anti IGF-IRα (SC-463, 1:50, Santa Cruz Biotechnology) or anti Flag M2 (F1804, 1:1000, Sigma-Aldrich) and secondary antibody Alexa Fluor 488 (A-11008, 1:1000, Life Technologies), and fixed before assessing fluorescence intensity by flow cytometry (FACS Aria, BD).

Cell surface protein biotinylation

Cell surface proteins were biotinylated following the manufacturer´s instructions (EZ-Link™Sulfo-NHS-SS-Biotin, Thermo Scientific). Biotinylated proteins were purified by affinity chromatography using NeutroAvidinAgarose Resin (Thermo Scientific) and resolved by Western blot. The membrane protein Na^+/K^+ ATPase was used as a loading control.

Quantitative PCR

Total RNA isolation from cell lysates or brain tissue was carried out with Trizol. One µg of RNA was reverse transcribed using High Capacity cDNA Reverse Transcription Kit (Life Technologies) according to the manufacturer's instructions. For quantification of specific genes, total RNA was isolated and transcribed as above and 62.5 ng of cDNA was amplified using TaqMan probes for GLUT1, GluT4, IGF-IR or IR, and 18S as endogenous control (Life Technologies). Each sample was run in triplicate in 20 µl of reaction volume using TaqMan Universal PCR Master Mix according to the manufacturer's instructions (Life Technologies). All reactions were performed in a 7500 Real Time PCR system (Life Technologies). Quantitative real time PCR analysis was carried out as described (Pfaffl 2001). Results were expressed as relative expression ratios on the basis of group means for target transcripts versus reference 18S transcript. At least three independent experiments were done.

Lentiviral particles administration

Mice were anesthetized by inhalation of a mixture of isofluorane/oxygen (5% induction, 2% maintenance). After removing the duramater, the tip of the glass pipette was placed onto the surface of the brain. Two µl of lentiviral shRNA against IGF-I receptor (~$4x10^{10}$ pfu/ml) were administered per mouse. Administration was made through a glass pipette connected to a Hamilton syringe. Rate of infusion was 1µl per 10 min. Stereotaxical coordinates were -1.06mm from bregma and -1mm lateral.

***In vivo* astrocyte glucose uptake**

Glucose uptake by astrocytes was evaluated as previously described by others (Chuquet et al., 2010) according to the experimental set-up shown in Suppl Figure 1A, following procedures described in detail elsewhere (Perez-Alvarez et al. 2013). Astrocytes were labelled with sulforhodamine 101 (100 mg/kg, i.p. SR101; Sigma-Aldrich). Mice were anesthetized with urethane (1.7g/kg, i.p. Sigma-Aldrich) and their femoral artery cannulated. A 4 mm craniotomy around the area of interest was made. After 5 min, the cortex was washed and a drop of low melting point agarose (1% in HEPES-buffered solution. Sigma-Aldrich) and a 5 mm glass coverslip were placed carefully over the exposed cortex. Dental cement (Fortex, Facident, Spain) was applied to fix the coverslip. A light aluminum frame (2x3.5cm) with a central circular hole (10mm diameter) was attached to the skull centered on the craniotomy area and fixed with dental cement. The cranial frame was fixed to a heavy aluminum base. The base was moved to the imaging stage. The animals' body temperature was monitored during the procedure using a rectal probe (Technomed Europe, The Netherlands) and regulated using a heating pad (RS Amidata, Spain) controlled by a thermostat (Cibertec, Spain) set at 37°C.

6-NBDG administration

6-NBDG (Setareh biotech, USA) was dissolved in a solution of 55% of HEPES-ringed buffer and 45% of DMSO, pH 7.42, to a concentration of 5 mg/ml. A 300µl Hamilton syringe (Hamilton, USA) filled with the 6-NBDG solution was connected to the femoral artery cannula and placed in a micro-injector pump (Harvard Apparatus, USA). 6-NBDG was pumped at a rate of 20µl/min/100gr.

Stimulation Paradigm

The whiskers of the animal's snout were stimulated with 100 ms puffs of air produced at 5 Hz by a pressure injector (Dagan, USA) for 30 sec controlled by an Axon Digidata 1322A and

pClamp software (Molecular Devices, USA). Air was ejected at 1 bar pressure via capillary glass, attached to plastic tubing, positioned ~1 cm lateral and anterior to the animal's nose to stimulate the whole left whisker pad. At the same time, tail pinching was performed at 2 Hz with steel forceps, providing a pairing protocol for astrocyte stimulation.

Laser Scanning Confocal Microscopy (LSCM)

Imaging was performed with a custom-built confocal laser (CVI Melles Griot, UK) scanning microscope consisting of an Olympus FV300 laser scanning confocal system coupled to an Olympus BX61WI upright microscope (Olympus, Japan) and a Olympus LUMPLFL 60XW/IR water immersion objective (0.9NA; Olympus)

Data analysis

Astrocytes were distinguished by using the red signal emitted by SR-101. Astrocytes concentrate SR-101, and their soma appear intensely bright (Nimmerjahn et al. 2004). Each image of the sequence was aligned over the previous image with Align Slice (ImageJ, National Institutes of Health, USA) to correct x–y deviation caused by possible drift of the tissue. Fluorescence intensity was measured in a region of interest (ROI) strictly limited to the somatic area. Signals were expressed as relative fluorescence changes ($\Delta F/F0$), where F0 was the mean of the baseline period. Astrocytes showing variations greater than 1 were considered as responders.

^{18}F-FDG PET imaging

^{18}F-FDG PET was used to measure brain glucose handling. Briefly, fasted mice were injected i.p. with the positron emitting radiotracer ^{18}F-FDG (18.5 MBq in 0.2 ml of 0.9% NaCl, Instituto Tecnológico PET, Spain). During an uptake period of 45 min animals were anesthetized by inhalation of a mixture of isoflurane/oxygen (5% for induction and 2% for maintenance) and then placed on the bed of the tomograph. The duration of the PET acquisition was 20 min, immediately followed by a CT (computed tomography) scan. The scanner used was a specific small animal PET-CT hybrid tomograph (Albira ARS, Oncovision, Spain). After acquisition, PET images were reconstructed with an ordered subset expectation maximization (OSEM) algorithm, and with applied corrections for randoms, scatter, attenuation, dead time and radio element decay, whereas for the CT images a filtered back projection algorithm was used. For metabolic activity quantification, the procedure used was as follows: first, the CT image of the skull from each animal was co-registered to a magnetic resonance image (MRI) template of

mouse brain in which the regions of interest (ROIs) were previously delineated. After the CT image was co-registered, the spatial mathematic transformation was saved and then applied to its own fused PET image, allowing the correct matching between the PET image and the MRI template. Once the ^{18}F-FDG uptake in the different brain regions was calculated (in kBq/cc units), the activity of each left hemisphere region was normalized to its homologous region in the right hemisphere and expressed as proportional uptake (left/right). All processes of visualization, co-registration and quantification were performed using PMOD 3.0 software (PMOD Technologies Ltd., Switzerland).

Statistics

Normal distribution tests were carried out in all initial set of experiments and a non-parametric Wilcoxon test was applied accordingly. For samples with normal distribution, parametric tests include one-way ANOVA followed by a Tukey HSD or t-test. A $p<0.05$ was considered significant. Results are shown as mean ± s.e.m. No statistical methods were used to predetermine sample sizes. Data collection and analysis were performed blinded to the conditions of the experiments only in *in vivo* experiments. There was no randomization of data collection or processing.

Results

IGF-IR in astrocytes modulates brain glucose uptake

We first examined whether IGF-IR affects brain glucose handling by reducing its levels with shRNA interference and measuring brain glucose uptake with ^{18}F fluoro-2 deoxy-glucose micro-PET imaging. A lentiviral vector expressing IGF-IR shRNA (Suppl Figure 1A) was stereotaxically injected into one side of the somatosensory cortex of wild type mice, whereas the contralateral side was injected with scrambled shRNA (Suppl Figure 1B), using procedures already described in detail elsewhere (Carro et al. 2005). After measuring baseline levels, we stimulated the whiskers bilaterally to increase glucose flux into the somatosensory cortex. Whereas glucose uptake was increased in both sides after whisker stimulation (Suppl Figure 1C), normalization of glucose levels in the side injected with IGF-IR shRNA with those in the scramble-injected side, both under basal conditions and after stimulation of the whiskers, revealed a significantly greater increase in glucose uptake after stimulation (Figure 1). No changes in glucose uptake were seen in a brain area such as the caudate-putamen that is not

activated after whisker stimulation. Despite the limitations of PET analysis in small animals such as mice (Kuntner et al. 2009), these results indicate that reducing brain IGF-IR enhances brain glucose uptake in active brain regions.

Because it has been shown that astrocytes are the predominant type of cell involved in glucose uptake upon activation of the somatosensory cortex (Chuquet et al. 2010), we used in vivo fluorescence microscopy (Suppl Figure 2) to visualize astrocytes in mice injected with IGF-IR shRNA in the somatosensory cortex, using procedures already described (Perez-Alvarez et al. 2013). We found significantly larger increases after stimulation of the whiskers in glucose transport (detected with 6-NBDG) in somatosensory cortex astrocytes (identified with the astrocyte-specific fluorescent red marker SR101) injected with IGF-IR shRNA, as compared to scramble RNA-injected astrocytes (Figure 2B-D and supplementary video).

As injection of the lentiviral particles transducing IGF-IR shRNA in the brain affected all types of brain cells, we needed to confirm whether IGF-IR in astrocytes was involved in glucose uptake, Thus, we performed PET analysis in mice with reduced IGF-IR specifically in astrocytes (As IGF-IR$^{+/-}$). Compared to littermates, a significant increase in glucose uptake in somatosensory cortex after sensory stimulation was seen in As IGF-IR$^{+/-}$ mice (Figure 2D). PET analysis was performed in heterozygous mice (As IGF-IR$^{+/-}$) because homozygous mice (As IGF-IR$^{-/-}$) have reduced brain size (not shown). Astrocytes from As IGF-IR$^{+/-}$ mice showed reduced responses to IGF-I (1 nM), as determined by phosphorylation of Akt (Suppl Figure 3A), even though total brain levels of IGF-IR were not significantly reduced in these mice, as many other brain cells express IGF-IR (Suppl Figure 3B).

Opposing action of IR and IGF-IR on GLUT1 activity in astrocytes

We then examined mechanisms whereby IGF-IR reduces glucose transport using astrocyte cultures. We first confirmed that reduction of IGF-IR in shRNA IGF-IR-transfected astrocytes significantly increased glucose transport (Figure 3A). Because astrocytes also express IR (Suppl Figure 4A), we also tested its role on glucose transport. Intriguingly, reduction of IR levels (Suppl Figure 4B) decreased glucose transport in astrocytes (Figure 3A). Opposing actions of IR and IGF-IR on glucose transport were confirmed by the observation that when both receptors were reduced, the effects cancelled each other (Figure 3A). Modulation of basal glucose transport in astrocytes after reduction of either IR or IGF-IR reflects ligand-independent actions

of these receptors (Boucher et al. 2010), as experiments were conducted under serum-free conditions, and addition of either IGF-I or insulin in the presence or absence of the respective shRNAs did not alter glucose transport in any case (not shown).

Because GLUT1 is the main facilitative glucose transporter in astrocytes (Morgello et al. 1995), we determined its role in IGF-IR and IR actions. We found that decreasing IR levels reduced GLUT1 mRNA (Figure 3B), resulting in decreased GLUT1 levels at the cell membrane (Figure 3C). Confirming these observations in vitro, we also found reduced levels of brain GLUT1 mRNA in mice lacking IR in astrocytes (GFAPIR-KO mice, Figure 3D). Indeed, GFAPIR-KO mice show wide disturbances in brain glucose handling, as reported elsewhere (Garcia-Caceres et al, in press). Thus, astrocytic IR modulates GLUT1 expression, and consequently GLUT1 protein levels at the cell membrane are also affected. On the other hand, reduction of IGF-IR by shRNA did not affect GLUT1 mRNA levels (Figure 3B), but resulted in increased amounts of GLUT1 at the cell membrane of astrocytes, as determined by flow cytometry and membrane protein biotinylation (Figure 3C,E). The latter suggests that IGF-IR retains GLUT1 inside the cell and agrees with the observation that reduction of IGF-IR levels increases glucose transport in astrocytes.

We then started to determine possible underlying mechanisms. IGF-IR associates with GIPC (GAIP-interacting protein, C terminus) (Booth et al. 2002; Bunn et al. 1999), a scaffolding protein that participates in protein trafficking and binds to many partners, including GLUT1 (Bunn et al. 1999). We hypothesized that GIPC may simultaneously interact with IGF-IR and GLUT1 through its PDZ domain because GIPC can dimerize (Katoh, 2013). In support of this possibility we found that IGF-IR co-immunoprecipitates not only with GIPC, as already reported, but also with GLUT1, whereas GIPC, as expected, co-immunoprecipitates also with GLUT1 (Figure 4A). Proximity ligation assays (PLA) confirmed an interaction between IGF-IR and GLUT1 (Figure 4B). Significantly, neither GLUT1, or as previously shown (Ligensa et al. 2001), nor GIPC, co-immunoprecipitate with the insulin receptor (Figure 4A). To further establish a role of GIPC in the interaction between IGF-IR and GLUT1 we reduced GIPC levels in astrocytes using GIPC shRNA (Suppl Figure 4C) and found that the interaction between IGF-IR and GLUT1 was significantly reduced (Figure 4C).

We examined a potential intermediary role of lipoprotein-receptor associated protein 1 (LRP1) in this mechanism as LRP1 is a multicargo membrane protein that associates to the IGF-I

receptor in other type of brain cells (Nishijima et al., 2010) and is involved in GLUT translocation in neurons (Liu et al. 2015). We confirmed that LRP1 and IGF-IR interact also in astrocytes (Suppl Figure 4D), and that LRP1 is required for IGF-IR to interact with GLUT1 and GIPC as its reduction with shRNA (Suppl Figure 4E) reduces the amount of IGF-IR that immunoprecipitates with GLUT1 and GIPC (Figure 4D). No direct interaction of LRP1 with GLUT1 was observed (Suppl Figure 4F).

Discussion

The present observations indicate that IGF-IR regulates glucose transporter 1 activity in astrocytes, impacting in this way on overall brain glucose transport. When IGF-IR levels are reduced, GLUT1 locates at the cell membrane and transports glucose inside the cell. Thus, unbound GLUT1 may contribute to basal glucose transport in astrocytes. Conversely, when GLUT1 is bound to IGF-IR, it remains inside the cell and associates to IGF-IR through protein-protein interactions involving GIPC and LRP1 (see Summary Graphic). As a facilitative glucose transporter, GLUT1 takes up extracellular glucose in a concentration-dependent manner, which explains increased glucose transport in shRNA IGF-IR-injected mice receiving sensory stimulation. Indeed, local blood flow is increased in response to enhanced neuronal activity (Roy and Sherrington 1890), and astrocytes, that fully wrap blood vessels (Mathiisen et al. 2010), will take up more glucose through GLUT1. In turn, previous observations indicate that activity-dependent modulation of astrocytic glucose transport relies on stimulation of GLUT1 by glutamate via engagement of the Na^+-glutamate co-transporter and intracellular Na^+-Ca^{++} co-signaling (Loaiza et al. 2003; Porras et al. 2008). Collectively, these observations provide additional information about the role of astrocytic GLUT1 in brain glucose metabolism.

In its IGF-IR-free state, GLUT1 is in the membrane and may be active. In this regard, and not withstanding different sensitivities of the methods used, the increase in glucose transport seen in astrocytes with reduced levels of IGF-IR is more robust that the increase seen in membrane GLUT1 levels. This could mean that the intrinsic activity of GLUT1, that can be regulated (Barnes et al. 2002), is also affected by IGF-IR. Thus, when associated to IGF-IR, GLUT1 is retained inside the cell and its activity is down-regulated. Bound and unbound GLUT1 may constitute two separate pools in astrocytes. We also speculate that when bound to IGF-IR,

GLUT1 may become subject to regulation by extracellular signals (glutamate…etc), but further work is needed.

This study confirms the utility of 6NBDG as a probe for glucose uptake, further supporting the notion that astrocytes are major contributors in glucose metabolism, as seen previously both in vivo (Chuquet et al. 2010), and in different in vitro preparations (Barros et al. 2009b; Jakoby et al. 2014). Importantly, both in anesthetized animals and in slices without anesthetics, 6NBDG showed preferential astrocytic uptake. Another important aspect confirmed by our findings is that IR and IGF-IR display ligand-independent activities that may, or may not, be related to the actions of their ligands (Boucher et al., 2010). In this regard, different authors have shown that IGF-I and insulin also affect glucose handling by astrocytes at different levels, including enhanced glucose uptake (Kum et al. 1992; Masters et al. 1991) and/or enhanced glycogen production (Dringen and Hamprecht 1992; Hamai et al. 1999; Muhic et al. 2015). These observations suggest that insulin peptides and their receptors form an intricate glucose regulatory network in astrocytes that may even act in apparently opposing manners. Indeed, and through entirely different mechanisms, IGF-IR exerts an intrinsic inhibitory action on astrocytic glucose transport, while IR displays an intrinsic stimulatory activity. In this way, glucose uptake in astrocytes may in part be determined by a balance between IGF-IR and IR levels. This suggests that physiological and pathological processes impacting on astrocytic insulin and IGF-I receptor levels will influence glucose transport by the brain in opposite directions.

Collectively, these observations would help reconcile the apparent controversy on the role of these receptors and their ligands in the brain (Cohen and Dillin 2008), which largely arises from studies in invertebrates harboring a single insulin-like receptor (Kenyon 2010). Thus, while in C *elegans* a single insulin-like receptor is modulated by many different ligands, even in an antagonistic fashion (Matsunaga et al. 2012), the acquisition of new insulin-like receptors in vertebrates has allowed the appearance of interactions among them. Based on present findings we consider that reported actions of insulin-like receptors in invertebrates should not be immediately inferred to be similar in vertebrates. The corollary of these observations is that invertebrate models of insulin-like receptor physiology in mammals should take into account the existence of two tyrosine kinase receptors, IGF-IR and IR, not present in invertebrates that may display cooperative (Boucher et al., 2010) or opposing activities (present observations), depending on biological context.

Finally, since glucose transport by the brain deteriorates during aging and its associated pathologies (Mergenthaler et al. 2013), these observations provide further support for the use of strategies regulating brain IGF-IR levels to support healthy as well as pathological aging. Indeed, lowering IGF-IR in Alzheimer´s disease (AD) brains will not only diminish amyloidosis (Cohen et al. 2009), and related pathology such as hippocampal hyperactivity (Gazit et al. 2016), but will also likely contribute to normalize glucose dysregulation present as a characteristic alteration of this disease (La Joie et al. 2012). Future work should examine major components of the IGF-IR pathway in astrocytes described herein for brain glucose regulation in experimental models of normal and pathological aging, as for example the recently described role of GLUT1 in AD (Winkler et al. 2015). Altogether, these set of observations support a role of an interaction between insulin and IGF-I receptors in modulating glucose handling by astrocytes, adding a new layer of regulation by astrocytes of brain energy economy (Allaman et al. 2011).

Competing interests

The authors declare no competing interests.

Author´s contributions

E HG and AM F designed and performed in vivo and in vitro experiments and analyzed results. APA performed experiments of confocal microscopy and analyzed results. LG performed in vitro experiments in astrocytes and characterize mutant mice. PB, RFR and MD performed PET experiments. MAP analyzed PET results. EM performed PLA experiments. PJM designed and performed PLA experiments. AS and ATS performed in vitro experiments in astrocytes CGC performed in vivo experiments with Glut. MT designed and analyzed in vivo experiments with Glut1. AA designed confocal microscopy experiments. EDM designed and performed confocal experiments. ITA designed the study and wrote the manuscript

Acknowledgements

We are thankful to M. Garcia, M Dominguez, and L Guinea for technical support. E. Hernandez was partially funded by a fellowship from ColFuturo. This work was funded by grants SAF2013-40710-R and by CIBERNED.

LEGENDS TO FIGURES

Figure 1: IGF-IR inhibits brain glucose handling. Adult mice were unilaterally injected with lentival particles expressing shRNA IGF-IR (n=5) in one side of the somatosensory cortex and with scramble shRNA-expressing viral particles in the contralateral side (see Suppl Fig 1B). After allowing 2 weeks of recovery, animals were submitted to PET scans, and after basal (white bars) measurements of ^{18}F-FDG uptake they were bilaterally stimulated (black bars) +in their whiskers. Basal and stimulated responses in the shRNA IGF-IR injected site were normalized to responses in the scramble injected side. Significantly enhanced uptake in the somatosensory cortex injected with shRNA IGF-IR was seen in response to whisker stimulation. No changes were appreciated in a unstimulated area such as the caudate putamen, that was analyzed to determine region specificity in glucose responses to sensory stimulation (*$p<0.05$ vs basal). Lower panel: representative PET images under basal conditions and after whisker stimulation are shown. Greater signal (red) is seen after stimulation.

Figure 2: IGF-IR inhibits astrocyte glucose transport in vivo. A, Representative 6-NBDG fluorescence traces of astrocytes of somatosensory cortex after scramble (left) or IGF-IR shRNA (right) injection in the somatosensory cortex. **B,** Representative confocal images of astrocytes (red, left image) accumulating 6NBDG (green, middle image) during whisker stimulation (see Suppl video for a full temporal sequence). Three astrocytes are indicated with arrowheads, two of them accumulate more 6-NBDG as shown in the merged image (right). Astrocytes were stained with the specific astrocyte dye SR101 administered by intraperitoneal injection whereas glucose transport was determined using the green fluorescent analog 6-NBDG delivered by intra-femoral artery injection. **C,** Mice injected with IGF-IR shRNA showed no changes in the number of responding astrocytes (left histograms) but displayed a great increase in glucose transport (measured as amplitude of the fluorescence response of 6-NBDG; right histograms, n= 139; ***$p<0.001$ vs scramble shRNA; n= 123). **D,** While baseline (white bars) brain glucose transport in somatosensory cortex of mice with knock down of IGF-IR in astrocytes (IGF-IR$^{+/-}$) was similar to littermates, upon whisker stimulation significantly larger brain glucose transport was seen. (*$p<0.05$ vs basal and ##$p<0.05$ vs basal and vs stimulated littermates; n=6 per group).

Figure 3: Role of IGF-IR and IR on *in vitro* glucose transport by astrocytes. A, Depletion of IGF-IR in astrocytes by shRNA interference increases basal transport of 6-NBDG (n=6; ***p<0.001 vs scramble-transfected astrocytes). Depletion of IR by shRNA interference elicits the opposite effect: a decrease in basal transport of 6-NBDG (n=6; ***p<0.001 vs scramble-transfected astrocytes). Interference of both IR and IGF-IR in astrocytes results in abolition of the effects of each other and no changes in 6-NBDG transport (n=6). **B,** Depletion of IR, but not IGF-IR by shRNA interference decreases the amount of GLUT1 mRNA as determined by qPCR (n=3; ***p<0.001 vs scramble-transfected astrocytes). **C,** Reduction of IGF-IR increased the amount of GLUT1 in the cell membrane whereas depletion of IR decreased it (n=4; ***p<0.001, and *p<0.05 vs respective scramble). **D,** Brain levels of GLUT1 mRNA are significantly reduced in mice lacking insulin receptors in astrocytes (GFAPIR-KO), as compared to control littermates (**p<0.01 vs littermates; n=4). **E,** Increased cell surface levels of GLUT1 after transfection of astrocytes with shRNA for IGF-IR seen by flow cytometry (panel C), were confirmed by cell surface biotinylation assays. Cell membrane fraction was confirmed by the presence of the cell membrane protein Na^+/K^+ ATPase.

Figure 4: Role of GLUT1 on IGF-IR effects on cultured astrocytes. A, Analysis of interactions of IGF-IR with GLUT1 and GIPC using reciprocal immunoprecipitations and sequential blotting show that the 3 proteins interact with each other whereas only IGF-IR interacts with IR. Drawing: proposed interaction of GLUT1 with IGF-IR through GIPC. **B,** Proximity ligation assays (PLA) in astrocyte cultures show an interaction of IGF-IR with GLUT1 (red dots in left micrograph) that is absent when the IGF-IR antibody is omitted (Control). DAPI staining of astrocyte nuclei in blue. Bars are 20µm. **C,** Reduction of GIPC1 with shRNA interference resulted in significantly less IGF-IR bound to GLUT1. Representative blot and quantitation bars are shown (n=4; **p<0.01). **D,** Reduction of LRP1 levels in astrocytes by shRNA reduces the interaction of GLUT1 and GIPC with IGF-IR.

Summary Graphic: Schematic representation of IGF-IR/IR interactions with astrocytic GLUT1. When bound to IGF-IR, GLUT1 activity is reduced because IGF-IR retains it inside the cell through an interaction that involves the scaffolding protein GIPC and the transmembrane multicargo protein LRP1. When unbound, GLUT1 locates at the cell membrane, showing greater

sensitivity (illustrated as greater size) and glucose transport is increased. Thus, basal glucose transport by astrocytes will reflect the balance between IGF-IR-bound and –free GLUT1. In turn, IR favors the transcription of GLUT1 mRNA, resulting in increased levels of this transpoter at the cell membrane.

References

Allaman I, Belanger M, Magistretti PJ. 2011. Astrocyte-neuron metabolic relationships: for better and for worse. Trends Neurosci 34:76-87.

Barnes K, Ingram JC, Porras OH, Barros LF, Hudson ER, Fryer LG, Foufelle F, Carling D, Hardie DG, Baldwin SA. 2002. Activation of GLUT1 by metabolic and osmotic stress: potential involvement of AMP-activated protein kinase (AMPK). J Cell Sci 115:2433-42.

Barros LF, Bittner CX, Loaiza A, Ruminot I, Larenas V, Moldenhauer H, Oyarzun C, Alvarez M. 2009a. Kinetic validation of 6-NBDG as a probe for the glucose transporter GLUT1 in astrocytes. J Neurochem 109 Suppl 1:94-100.

Barros LF, Courjaret R, Jakoby P, Loaiza A, Lohr C, Deitmer JW. 2009b. Preferential transport and metabolism of glucose in Bergmann glia over Purkinje cells: a multiphoton study of cerebellar slices. Glia 57:962-70.

Biondi O, Branchu J, Ben Salah A, Houdebine L, ertin L, Chali F, Desseille C, eill L, Sanchez G, Lancelin C and others. 2015. IGF-1R Reduction Triggers Neuroprotective Signaling Pathways in Spinal Muscular Atrophy Mice. J Neurosci 35:12063-12079.

Booth RA, Cummings C, Tiberi M, Liu XJ. 2002. GIPC participates in G protein signaling downstream of insulin-like growth factor 1 receptor. J Biol Chem 277:6719-6725.

Boucher J, Macotela Y, Bezy O, Mori MA, Kriauciunas K, Kahn CR. 2010. A Kinase-Independent Role for Unoccupied Insulin and IGF-1 Receptors in the Control of Apoptosis. Sci Signal 3:ra87.

Bunn RC, Jensen MA, Reed BC. 1999. Protein interactions with the glucose transporter binding protein GLUT1CBP that provide a link between GLUT1 and the cytoskeleton. Mol Biol Cell 10:819-832.

Carro E, Spuch C, Trejo JL, Antequera D, Torres-Aleman I. 2005. Choroid Plexus Megalin Is Involved in Neuroprotection by Serum Insulin-Like Growth Factor I. J Neurosci 25:10884-10893.

Cohen E, Dillin A. 2008. The insulin paradox: aging, proteotoxicity and neurodegeneration. Nat Rev Neurosci 9:759-767.

Cohen E, Paulsson JF, Blinder P, Burstyn-Cohen T, Du D, Estepa G, Adame A, Pham HM, Holzenberger M, Kelly JW and others. 2009. Reduced IGF-1 signaling delays age-associated proteotoxicity in mice. Cell 139:1157-1169.

Chuquet J, Quilichini P, Nimchinsky EA, Buzsaki G. 2010. Predominant enhancement of glucose uptake in astrocytes versus neurons during activation of the somatosensory cortex. J Neurosci 30:15298-15303.

De Magalhaes Filho CD, Kappeler L, Dupont J, Solinc J, Villapol S, Denis C, Nosten-Bertrand M, Billard JM, Blaise A, Tronche F and others. 2016. Deleting IGF-1 receptor from forebrain neurons confers neuroprotection during stroke and upregulates endocrine somatotropin. J Cereb Blood Flow Metab. Pub ahead (accession number: 10.1177/0271678X15626718).

Dringen R, Hamprecht B. 1992. Glucose, insulin, and insulin-like growth factor I regulate the glycogen content of astroglia-rich primary cultures. J Neurochem 58:511-517.

Dull T, Zufferey R, Kelly M, Mandel RJ, Nguyen M, Trono D, Naldini L. 1998. A third-generation lentivirus vector with a conditional packaging system. J Virol 72:8463-71.

Fernandez AM, Fernandez S, Carrero P, Garcia-Garcia M, Torres-Aleman I. 2007. Calcineurin in reactive astrocytes plays a key role in the interplay between proinflammatory and anti-inflammatory signals. J Neurosci 27:8745-8756.

Fernandez AM, Torres-Aleman I. 2012. The many faces of insulin-like peptide signalling in the brain. Nat Rev Neurosci 13:225-239.

Gazit N, Vertkin I, Shapira I, Helm M, Slomowitz E, Sheiba M, Mor Y, Rizzoli S, Slutsky I. 2016. IGF-1 Receptor Differentially Regulates Spontaneous and Evoked Transmission via Mitochondria at Hippocampal Synapses. Neuron 89:1-15.

Gontier G, George C, Chaker Z, Holzenberger M, Aid S. 2015. Blocking IGF Signaling in Adult Neurons Alleviates Alzheimer's Disease Pathology through Amyloid-beta Clearance. J Neurosci 35:11500-11513.

Gonzalez S, Moreno-Delgado D, Moreno E, Perez-Capote K, Franco R, Mallol J, Cortes A, Casado V, Lluis C, Ortiz J and others. 2012. Circadian-related heteromerization of adrenergic and dopamine D(4) receptors modulates melatonin synthesis and release in the pineal gland. PLoS Biol 10:e1001347.

Hamai M, Minokoshi Y, Shimazu T. 1999. L-Glutamate and insulin enhance glycogen synthesis in cultured astrocytes from the rat brain through different intracellular mechanisms. J Neurochem 73:400-407.

Jakoby P, Schmidt E, Ruminot I, Gutierrez R, Barros LF, Deitmer JW. 2014. Higher transport and metabolism of glucose in astrocytes compared with neurons: a multiphoton study of hippocampal and cerebellar tissue slices. Cereb Cortex 24:222-31.

Kenyon CJ. 2010. The genetics of ageing. Nature 464:504-512.

Koshy S, Alizadeh P, Timchenko LT, Beeton C. 2010. Quantitative measurement of GLUT4 translocation to the plasma membrane by flow cytometr. J Vis Exp:pii: 2429. doi: 10.3791/2429.

Kum W, Zhu SQ, Ho SK, Young JD, Cockram CS. 1992. Effect of insulin on glucose and glycogen metabolism and leucine incorporation into protein in cultured mouse astrocytes. Glia 6:264-268.

Kuntner C, Kesner AL, Bauer M, Kremslehner R, Wanek T, Mandler M, Karch R, Stanek J, Wolf T, Muller M and others. 2009. Limitations of small animal PET imaging with [18F]FDDNP and FDG for quantitative studies in a transgenic mouse model of Alzheimer's disease. Mol Imaging Biol 11:236-240.

La Joie R, Perrotin A, Barros L, Hommet C, Mazenge F, Ibazizene M, Camus V, Abbas A, Landeau B, Guilloteau D and others. 2012. Region-Specific Hierarchy between Atrophy, Hypometabolism, and beta-Amyloid (Abeta) Load in Alzheimer's Disease Dementia. J Neurosci 32:16265-16273.

Ligensa T, Krauss S, Demuth D, Schumacher R, Camonis J, Jaques G, Weidner KM. 2001. A PDZ domain protein interacts with the C-terminal tail of the insulin-like growth factor-1 receptor but not with the insulin receptor. J Biol Chem 276:33419-33427.

Liu CC, Hu J, Tsai CW, Yue M, Melrose HL, Kanekiyo T, Bu G. 2015. Neuronal LRP1 Regulates Glucose Metabolism and Insulin Signaling in the Brain. J Neurosci 35:5851-5859.

Loaiza A, Porras OH, Barros LF. 2003. Glutamate triggers rapid glucose transport stimulation in astrocytes as evidenced by real-time confocal microscopy. J Neurosci 23:7337-42.

Lopez-Otin C, Blasco MA, Partridge L, Serrano M, Kroemer G. 2013. The Hallmarks of Aging. Cell 153:1194-1217.

Masters BA, Werner H, Roberts CT, Jr., LeRoith D, Raizada MK. 1991. Developmental regulation of insulin-like growth factor-I-stimulated glucose transporter in rat brain astrocytes. Endocrinology 128:2548-2557.

Mathiisen TM, Lehre KP, Danbolt NC, Ottersen OP. 2010. The perivascular astroglial sheath provides a complete covering of the brain microvessels: an electron microscopic 3D reconstruction. Glia 58:1094-103.

Matsunaga Y, Gengyo-Ando K, Mitani S, Iwasaki T, Kawano T. 2012. Physiological function, expression pattern, and transcriptional regulation of a Caenorhabditis elegans insulin-like peptide, INS-18. Biochem Biophys Res Commun 423:478-483.

Mergenthaler P, Lindauer U, Dienel GA, Meisel A. 2013. Sugar for the brain: the role of glucose in physiological and pathological brain function. Trends Neurosci 36:587-597.

Morgello S, Uson RR, Schwartz EJ, Haber RS. 1995. The human blood-brain barrier glucose transporter (GLUT1) is a glucose transporter of gray matter astrocytes. Glia 14:43-54.

Muhic M, Vardjan N, Chowdhury HH, Zorec R, Kreft M. 2015. Insulin and Insulin-like Growth Factor 1 (IGF-1) Modulate Cytoplasmic Glucose and Glycogen Levels but Not Glucose Transport across the Membrane in Astrocytes. J Biol Chem 290:11167-11176.

Munive V, Santi A, Torres-Aleman I. 2016. A Concerted Action Of Estradiol And Insulin Like Growth Factor I Underlies Sex Differences In Mood Regulation By Exercise. Sci Rep 6:25969.

Nimmerjahn A, Kirchhoff F, Kerr JN, Helmchen F. 2004. Sulforhodamine 101 as a specific marker of astroglia in the neocortex in vivo. Nat Methods 1:31-7.

Nishijima T, Piriz J, Duflot S, Fernandez AM, Gaitan G, Gomez-Pinedo U, Verdugo JM, Leroy F, Soya H, Nunez A and others. 2010. Neuronal activity drives localized blood-brain-barrier transport of serum insulin-like growth factor-I into the CNS. Neuron 67:834-846.

Perez-Alvarez A, Araque A, Martin ED. 2013. Confocal microscopy for astrocyte in vivo imaging: Recycle and reuse in microscopy. Front Cell Neurosci 7:51.

Pfaffl MW. 2001. A new mathematical model for relative quantification in real-time RT-PCR. Nucleic Acids Res 29:e45.

Porras OH, Ruminot I, Loaiza A, Barros LF. 2008. Na(+)-Ca(2+) cosignaling in the stimulation of the glucose transporter GLUT1 in cultured astrocytes. Glia 56:59-68.

Roy CS, Sherrington C. 1890. On the regulation of the blood supply of the brain. J Physiol 11:85-108.

Vilchez D, Saez I, Dillin A. 2014. The role of protein clearance mechanisms in organismal ageing and age-related diseases. Nat Commun 5:5659.

Wieman HL, Wofford JA, Rathmell JC. 2007. Cytokine stimulation promotes glucose uptake via phosphatidylinositol-3 kinase/Akt regulation of Glut1 activity and trafficking. Mol Biol Cell 18:1437-1446.

Winkler EA, Nishida Y, Sagare AP, Rege SV, Bell RD, Perlmutter D, Sengillo JD, Hillman S, Kong P, Nelson AR and others. 2015. GLUT1 reductions exacerbate Alzheimer's disease vasculo-neuronal dysfunction and degeneration. Nat Neurosci 18:521-530.

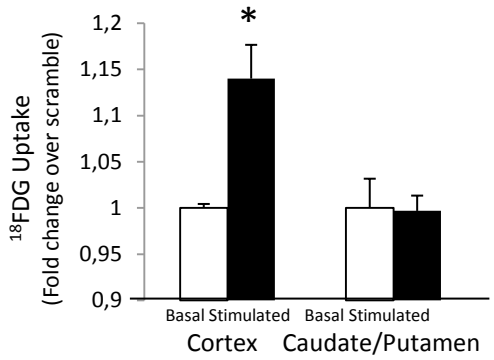

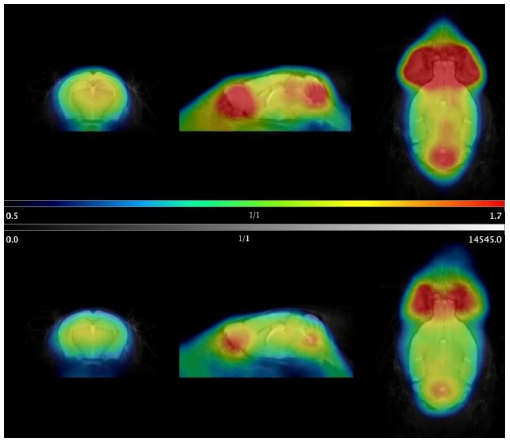

Stimulation

Basal

Figure 1

A

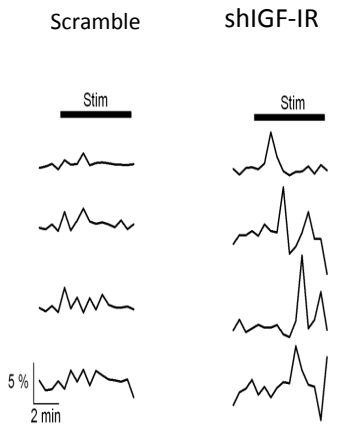

B

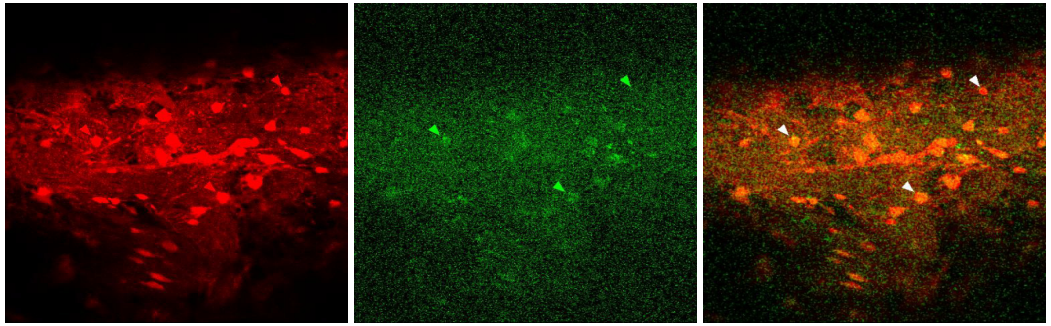

C

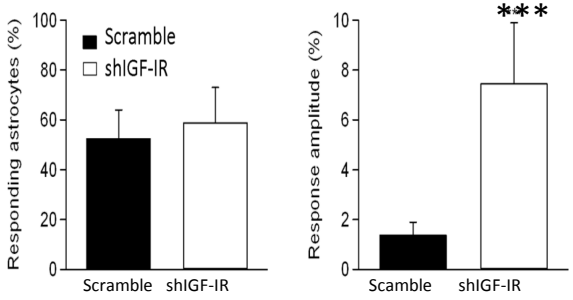

D

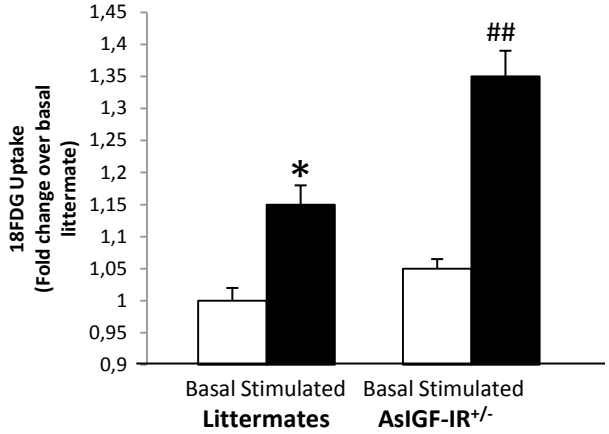

Figure 2

A

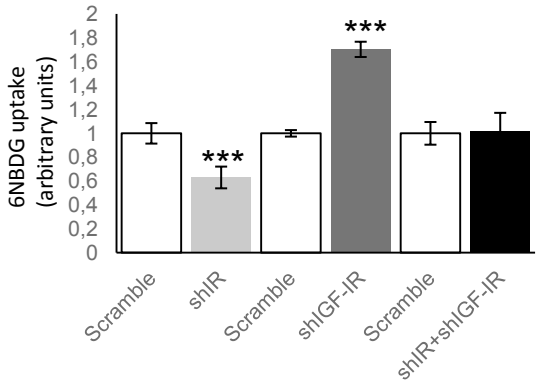

B

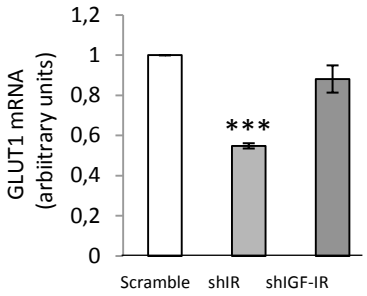

C

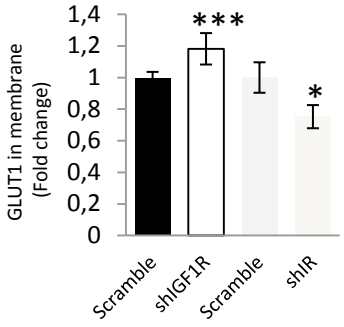

D

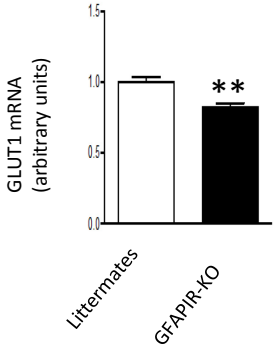

E

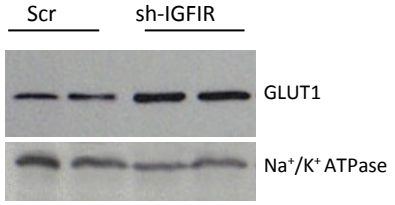

Figure 3

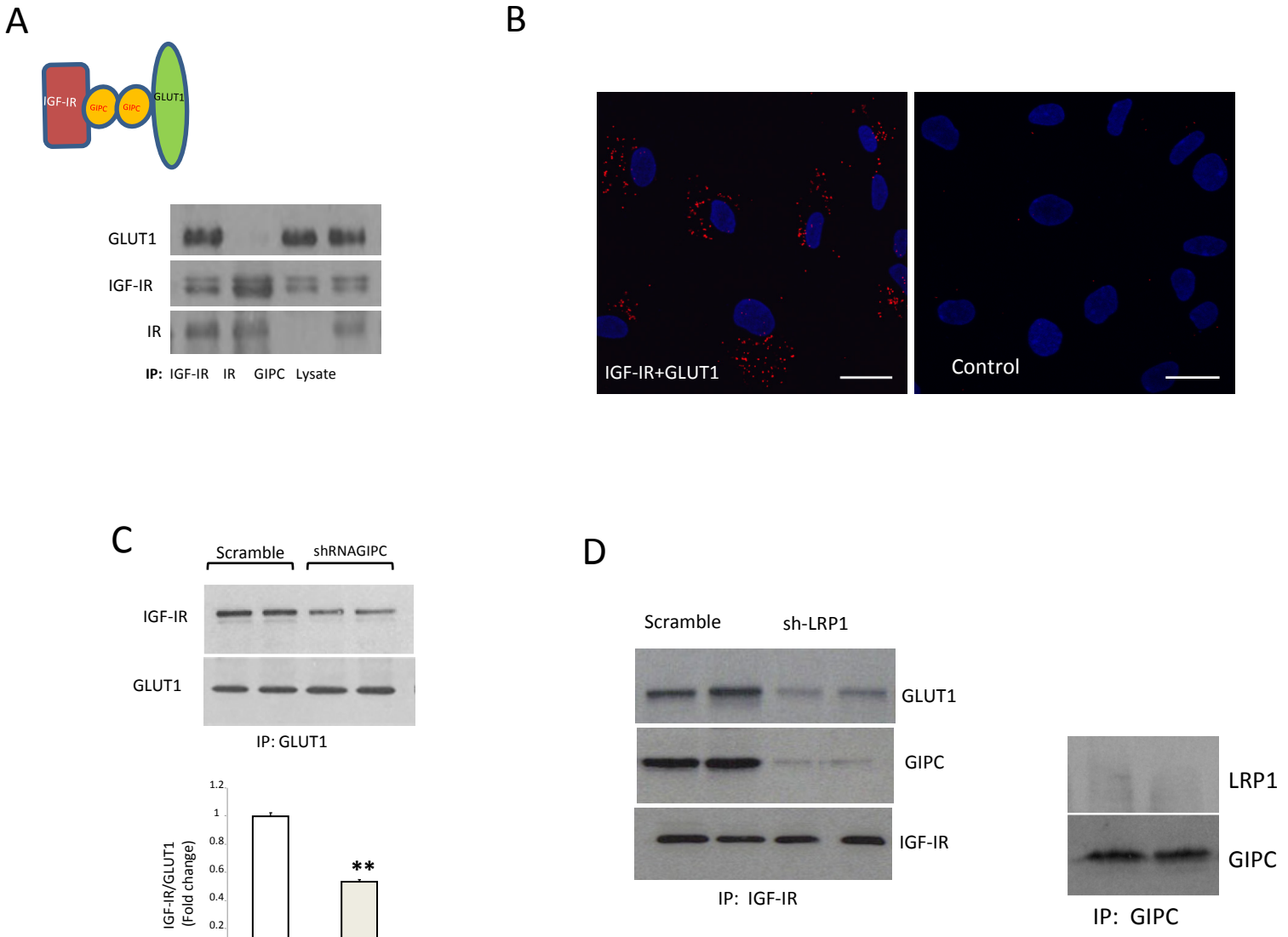
A
IGF-IR
GIPC
GIPC
GLUT1
GLUT1
IGF-IR
IR
IP: IGF-IR IR GIPC Lysate
B
IGF-IR+GLUT1
Control
C
Scramble
shRNAGIPC
IGF-IR
GLUT1
IP: GLUT1
IGF-IR/GLUT1 (Fold change)
1.2
1
0.8
0.6
0.4
0.2
0
**
Scramble
shRNAGIPC
D
Scramble
sh-LRP1
GLUT1
GIPC
IGF-IR
IP: IGF-IR
LRP1
GIPC
IP: GIPC

Figure 4

LEGENDS SUPPLEMENTARY FIGURES

Supplementary Figure 1. **A,** Three different shRNAs for IGF-IR were tested in cultured astrocytes. Number 88 was selected based on its greater potency. **B,** Adult mice were injected with lentival particles expressing shRNA IGF-IR in one side of the somatosensory cortex and with scramble shRNA-expressing viral particles in the contralateral side. Lower micrograph: a representative GFP staining of GFP-expressing control viral vectors is shown to illustrate the spreading of viral expression within the somatosensory cortex (Scx). The circled area depicts the region selected for microscopy analysis. Bar is 500 µm. Hi: hippocampus; CC: corpus callosum. No spreading of virus was seen in the contralateral side. **C,** PET analysis of glucose uptake in the somatosensory cortex showed that basal glucose uptake was slightly, but not significantly reduced in the side injected with shRNA IGF-IR compared to the scramble-injected side. After whisker stimulation both sides showed increased uptake, but the increase over basal levels was greater in the shRNA IGF-IR side. **D,** Three different shRNAs for IR were tested in cultured astrocytes. Number 30 was selected for experimental use.

Supplementary Figure 2. A, Time-line of experimental set-up for in vivo analysis of glucose transport by astrocytes. Animals received an ip injection of SR101 (100 mg/kg) immediately followed by ip urethane (1.7 g/kg). Once the animals were anesthesized**,** their femoral vein was cannulated and placed under the microscope. After a cranial window was opened and image stabilized, the animals were injected 6NBDG (see materials and methods for the detailed procedure) and recordings started. **B,** Schematic illustration of the positioning of the microscope over the cranial window of an anesthesized mouse. **C,** Left: representative image of somatosensory cortex astrocytes labeled with SR101; right micrograph: uptake of 6NBDG in the somatosensory cortex under basal conditions. Bar is 20 µm. **D,** Representative measurements of three SR101-labeled astrocytes (1, 2, and 3 in left image) accumulating 6NBDG before (middle image), and after (right image) somatosensory stimulation. Fluorescence traces are shown in the rightmost panel. Bar is 10 µm.

Supplementary Figure 3. **A,** In vitro responses to IGF-I (1 nM) in astrocytes derived from mice with knock down (AsIGF-IR$^{+/-}$) or knock out (AsIGF-IR$^{-/-}$) IGF-I receptors in astrocytes were proportional to the reduction in IGF-IR levels, as measured by Akt phosphorylation (n=3;

*p<0.05 vs control and #p<0.05 vs IGF-I in control astrocytes). **B,** Brain levels of IGF-IR in mice with IGF-IR knock out in astrocytes (As IGF-IR$^{-/-}$) were significantly reduced. Remaining IGF-IR is expressed by other brain cells.

Supplementary Figure 4. A, Astrocytes express both insulin (IR) and IGF-I (IGF-IR) receptors as determined by qPCR (n=6). Levels are expressed relative to IR. **B,** Three different shRNAs for IR were tested in cultured astrocytes. Number 30 was selected for experimental use. **C,** shRNA GIPC reduces protein levels of GIPC in transfected astrocyte cultures. **D,** LRP1 and IGF-IR co-immunoprecipitate in astrocyte lysates. Representative blot is shown. IP: IGF-IR. **E,** Transfection of astrocytes with shRNA against LRP1 reduces its levels in these cells. **F,** GIPC does not co-immunoprecipitate with LRP1 in astrocyte lysates. Representative blot.

Video. In response to whisker/tail stimulation, astrocytes (red) in somatosensory cortex increase glucose uptake (green). Stimulation is delivered at ~9 sec in the video sequence. Astrocytes were stained with the specific astrocyte dye SR101 administered by intraperitoneal injection whereas glucose uptake was determined using the green fluorescent analog 6-NBDG delivered by intra-femoral artery injection.

A

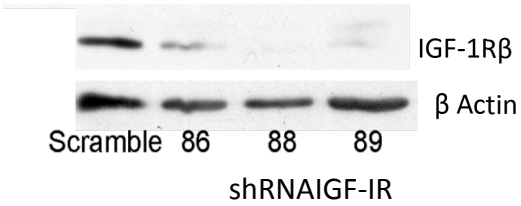

B

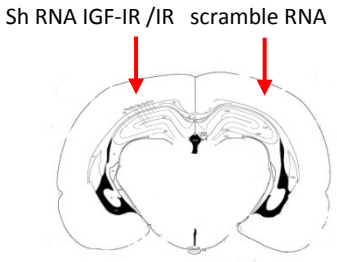

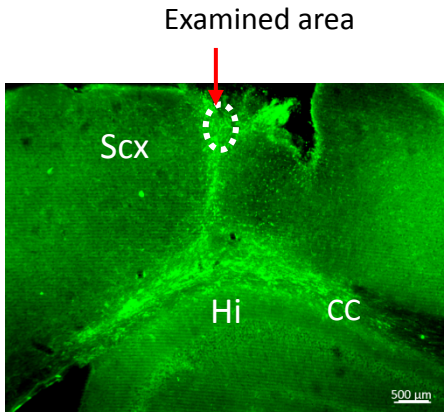

C

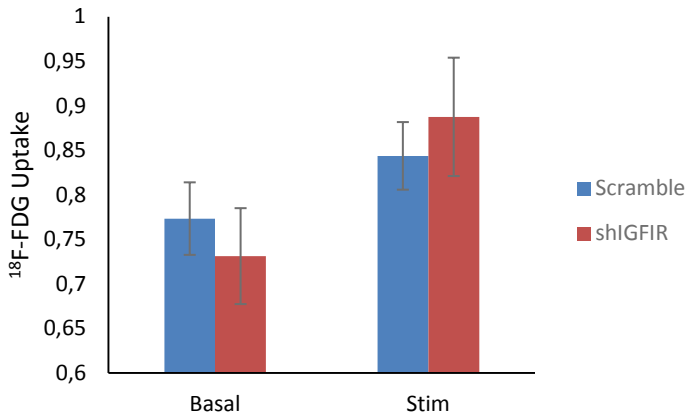

Supplementary Figure 1

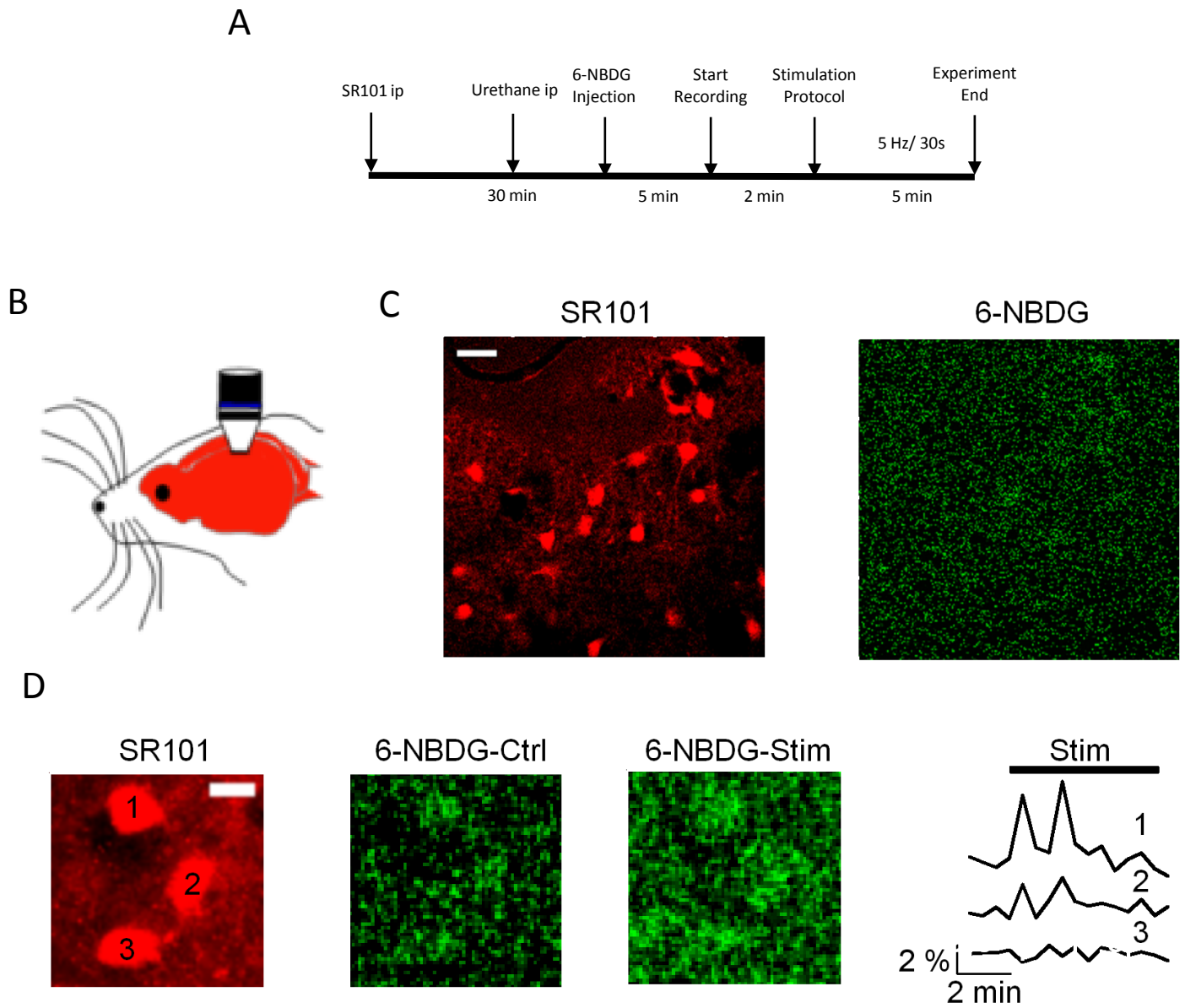

Supplementary Figure 2

A

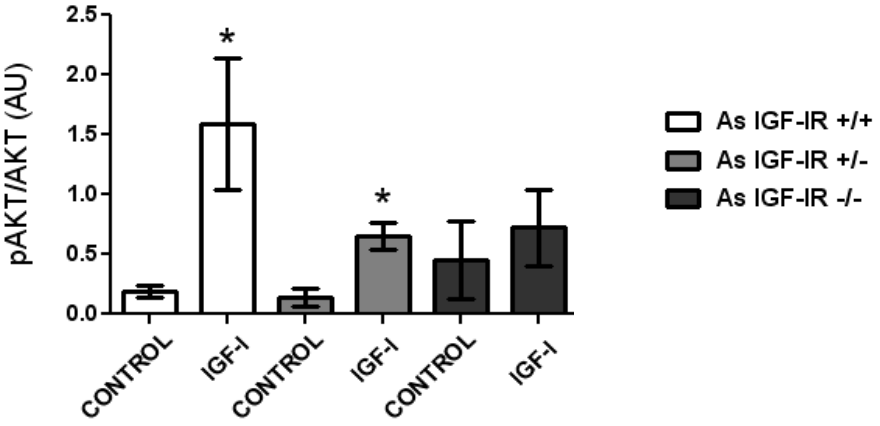

B

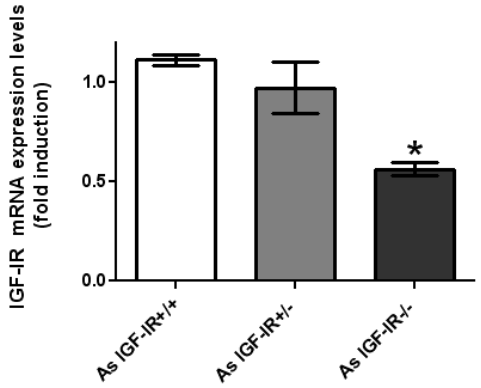

Supplementary Figure 3

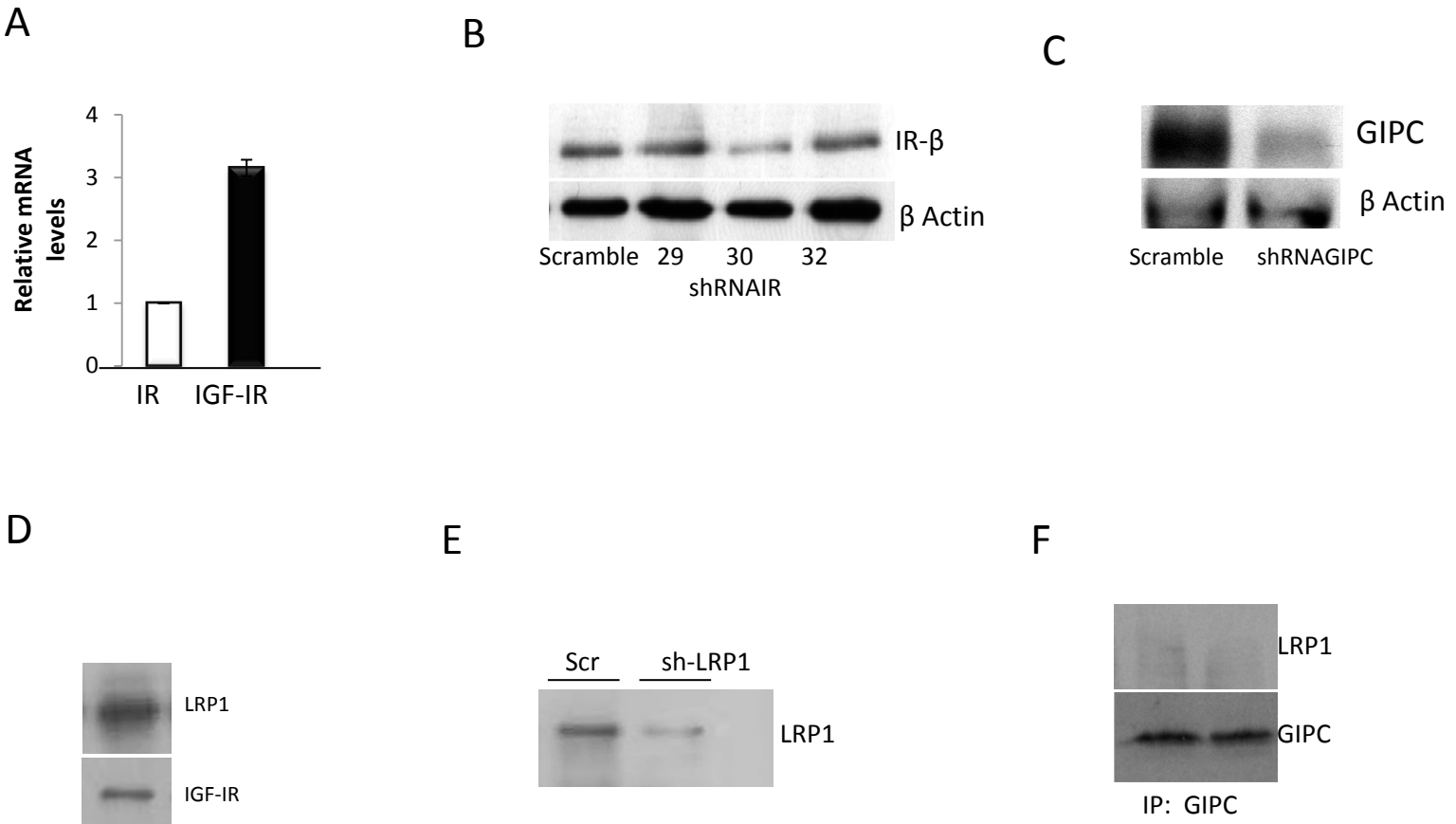

Supplementary Figure 4

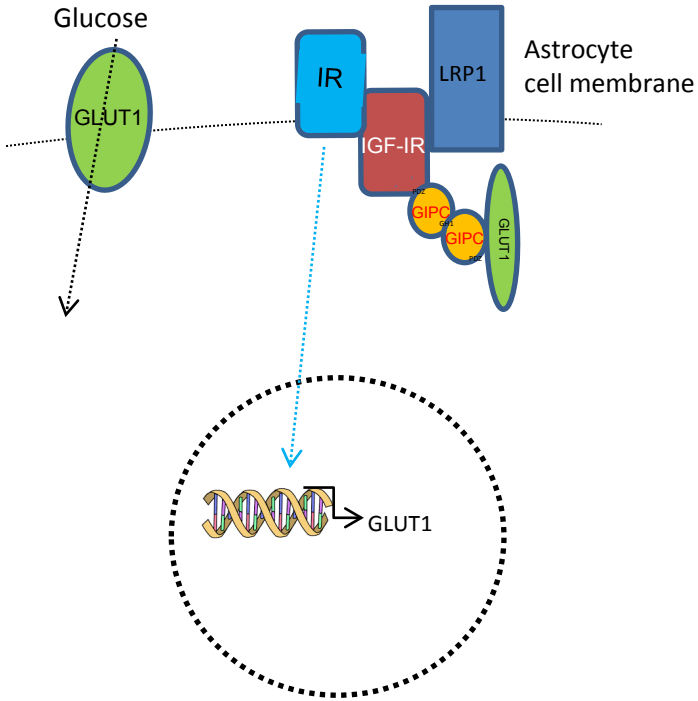

Summary Graphic